

Modelling and analysis of ship surface BRDF

David A. Vaitekunas^{a,1}

^aW.R. Davis Engineering Limited, 1260 Old Innes Road, Ottawa, Ontario, Canada K1B 3V3

Presented at the 2nd International Workshop on IR Target and Background Modelling & Simulation, 26–29 June 2006, FGAN-FOM Research Institute for Optronics and Pattern Recognition, Ettlingen, Germany

ABSTRACT

Modelling the bi-directional reflectance distribution function (BRDF) of a ship surface is an integral part of any infrared ship signature model. The ShipIR surface BRDF model is based on Sandford and Robertson (1985) and makes a discrete assumption for lobe-width and solar-glint. The ShipIR sea surface reflectance model uses a roughness model based on the early work of Cox and Munk (1954) and refined using the integral solution proposed by Mermelstein et al. (1994). A similar approach was used by Ward (1992) to model the visual properties of a real surface, considering isotropic and anisotropic surface roughness. This paper compares the two roughness models to show how bi-directional reflectance (sr^{-1}) is not ideally suited for modelling micro-faceted surface reflections. The simulation of an actual ship IR glint measurement demonstrates the effect of BRDF lobes in the paint property and provides a qualitative assessment of the ShipIR model.

Keywords: ship signature, infrared, bi-directional reflectance, surface roughness, modelling

1. INTRODUCTION

The NATO-standard and US-Navy accredited ship infrared signature model (ShipIR) has undergone extensive validation using field trial data from US Navy (Vaitekunas and Fraedrich, 1999) and Canadian Navy (Vaitekunas 2005, Vaitekunas 2004, Fraedrich et al. 2003) assets. Two important observations were made during the last round of model validation using ShipIR (v3.2). First, to further improve the ShipIR thermal model, background radiation from the horizon had to be measured in addition to that already collected for the down-welling sky. Second, a large portion of the error in the mid-wave (3–5 μm) ShipIR predictions for the Canadian Forces Auxiliary Vessel (CFAV) Quest was attributed to a lack of control (or measurement) of the optical surface properties of the Quest white and yellow paints. The first observation was incorporated into the planning of a NATO-sponsored IR measurement trial held recently in Chesapeake Bay (SAPPHIRE, 2006). Additional thermal and solar irradiance sensors were installed on Quest to measure the radiation from the horizon. The second observation and discussions that followed the 1st ITBM Workshop have resulted in the current work which describes some of the BRDF measurements and models used to predict the operational behaviour of ship surfaces. As shown in Figure 1, the mid-wave solar reflections off the Quest white paint provide an ideal opportunity for measurement and prediction of bi-directional reflectance. The objective of this paper is to define the ship surface BRDF based on existing optical surface measurements, review the reflectance models used by ShipIR and compare these with other models based on surface roughness, and then demonstrate the ability of ShipIR to reproduce an occurrence of IR solar-glint, as measured during the Quest Q280 trial in February 2004.

¹ davidv@davis-eng.com; <http://www.davis-eng.com>; phone: +1 613 748 5500; fax: +1 613 748 3972

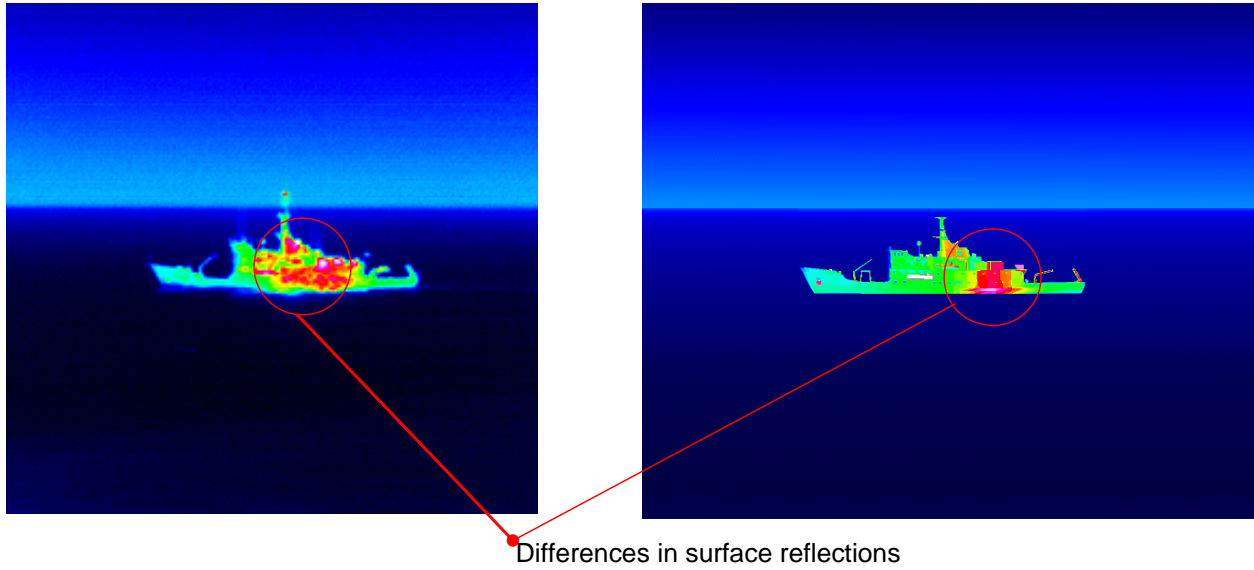


Figure 1: Comparison of measured (left) and predicted (right) infrared images of CFAV Quest during Q276 trial in August 2003.

2. SURFACE REFLECTANCE

The following section describes some standard definitions and measurement techniques used to characterize the thermal, optical and in-band properties of a surface coating. The definitions and sample measurements provide a basis on which to describe the ShipIR and other models of bi-directional reflectance. Two roughness-based reflectance models are introduced to show how micro-facets can be used to represent the large specular lobes associated with most navy paints.

2.1 Definitions

The first surface property to be defined is the bi-directional reflectance, which is the ratio between the reflected surface radiance (L_r) and the radiant flux associated with a small incident source (dE):

$$\rho_{bd} = \frac{L_r(\phi_r, \theta_r)}{dE_i} = \frac{L_r(\phi_r, \theta_r)}{L_i(\phi_i, \theta_i) \cos \theta_i \sin \theta_i d\phi_i d\theta_i} = f(\phi_i, \theta_i, \phi_r, \theta_r, \lambda) \quad (1)$$

Although this property is denoted by the common Greek symbol of reflectance (ρ), it has physical units (sr^{-1}) based on the following definition of a differential solid angle (sr) for a small angle source:

$$d\omega_i = \frac{dA_n}{r^2} = \frac{(r \sin \theta d\phi)(r d\theta)}{r^2} = \sin \theta_i d\phi_i d\theta_i \quad (2)$$

The next sub-section will show how bi-directional reflectance (ρ_{bd}) measurements are obtained using a goniometric reflectometer, and discuss whether this *artificial* definition of reflectance is useful in modelling surface radiance.

The next important surface property to be defined is the directional hemispherical reflectance (DHR), which is the fraction of the incident differential radiant flux being reflected in all directions:

$$\rho_{dh}(\phi_i, \theta_i) = \int_{\Omega_r} \frac{dE_r}{dE_i} = \int_0^{2\pi} \int_0^{\pi/2} \frac{L_r(\phi_r, \theta_r) \cos \theta_r}{L_i(\phi_i, \theta_i) \cos \theta_i} \sin \theta_r d\theta_r d\phi_r \quad (3)$$

After substituting for the bi-directional reflectance, we see that this property is simply a solid-angle integral of the bi-directional reflectance or BRDF²:

² Bi-directional Reflectance Distribution Function or BRDF is a family of curves or functions used to describe the bi-directional reflectance over a range of incident and reflected angles.

$$\rho_{dh}(\phi_i, \theta_i) = \int_0^{2\pi} \int_0^{\pi/2} \frac{L_r(\phi_r, \theta_r) \cos \theta_r \sin \theta_r d\theta_r d\phi_r}{L_r(\phi_i, \theta_i)} = \int_0^{2\pi} \int_0^{\pi/2} \rho_{bd}(\phi_i, \theta_i, \phi_r, \theta_r) \cos \theta_r \sin \theta_r d\theta_r d\phi_r \quad (4)$$

A similar property called hemispherical directional reflectance (HDR) can be obtained by carrying out the same integral, but for all incident angles:

$$\rho_{hd}(\phi_r, \theta_r) = \int_{\Omega_i} \frac{dE_r}{dE_i} = \int_0^{2\pi} \int_0^{\pi/2} \frac{L_r(\phi_r, \theta_r) \cos \theta_r \sin \theta_i d\theta_i d\phi_i}{L_r(\phi_i, \theta_i)} = \int_0^{2\pi} \int_0^{\pi/2} \rho_{bd}(\phi_i, \theta_i, \phi_r, \theta_r) \cos \theta_r \sin \theta_i d\theta_i d\phi_i \quad (5)$$

These two terms are commonly equated with the total or nominal reflectance of a surface when the corresponding incident source angle is small ($\theta < 30^\circ$).

2.2 Measurement

The following measurements were obtained from the CFAV Quest white and yellow paints. Some were measured by Surface Optics Corporation (SOC)³ during the Q280 measurement trial in 2004, while others were measured by the Norwegian Defence Research Establishment (FFI)⁴ during the NATO SIMVEX (Q262) trial in 2001. Figure 2 shows the hemispherical (HDR) and diffuse (DDR) directional reflectance of the Quest white paint as measured by SOC in the spectral range from 0.3 to 50 μm (200–33000 cm^{-1}) using an incident source angle of 20°. The diffuse component (DDR) is obtained using a *blocker* to absorb the reflected radiance in an area surrounding the centre of the specular lobe ($\phi_r = \phi_i + \pi$, $\theta_r = \theta_i$). These results show a high diffuse reflectance in the visual band (0.5–2.0 μm) typical for a white paint, and a high thermal emissivity in the long-wave thermal region ($\lambda > 5\mu\text{m}$) also typical of navy paints. The white Quest paint is particularly interesting for IR measurement and modelling because of its moderate reflectance (0.1–0.3) in the 3–4 μm band where the sun also emits. Although the specular component of the nominal reflectance is low (less than 10% across the spectrum), the value will increase at higher incident angles and accounts for 100% of the total reflectance at wavelengths greater than 8 μm .

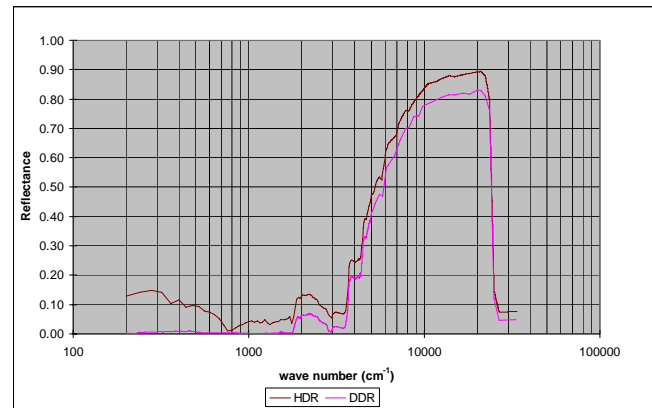


Figure 2: Hemispherical (HDR) and diffuse (DDR) directional reflectance versus wave-number (cm^{-1}) for the Quest white paint.

Figures 3 and 4 show bi-directional reflectance measurements taken from a navy-grey paint sample at 4 μm and 10 μm , respectively, using an incident source angle of 30°. Also shown are two BRDF model representations of the same data – one using the *SPECULAR* option of ShipIR (denoted as FWHM) and the other based on a roughness model similar to the one used for sea reflectance (denoted as PDF). These models are described in the following sub-sections. Figure 5 shows a series of spectral reflectance curves measured by FFI for the Quest white paint. These curves illustrate how specular reflectance increases with incidence angle, regardless of wavelength. Figure 6 shows a series of normalized reflectance data points obtained from the FFI measurements, and compares them with a least-square fit to the Sandford and Robertson (1985) model. Five different spectral groups sharing the same spectral profile were defined and used to fit the model. There are some obvious discrepancies in the data below 40°, where the nominal value (averaged from 0 to 30°) is larger than the data at 35°, but we assume this to be an artifact of the measurement and not a property of the surface.

³ Surface Optics Corporation, 11555 Rancho Bernardo Rd., San Diego, CA 92127. Phone: 858 675 7404 fax: 858 675 2028; www.surfaceoptics.com

⁴ Forsvarets forskningsinstitutt (FFI), Postboks 25 2027 Kjeller, phone: 63 80 70 00, fax: 63 80 71 15; www.mil.no

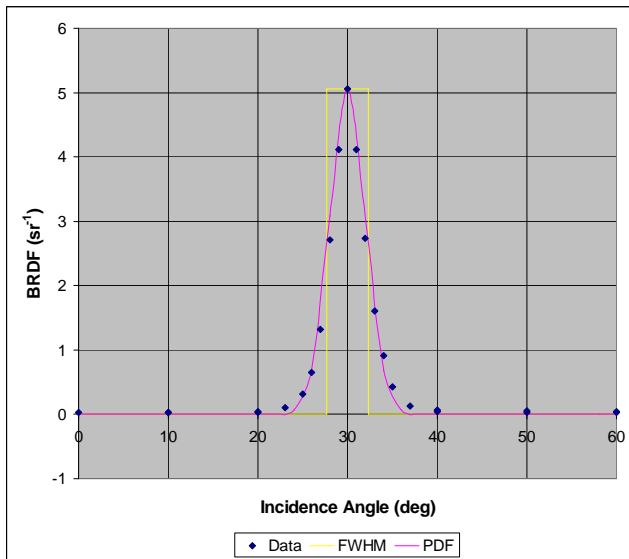


Figure 3: Bi-directional reflectance versus incidence for a 4µm source positioned in-plane at 30°.

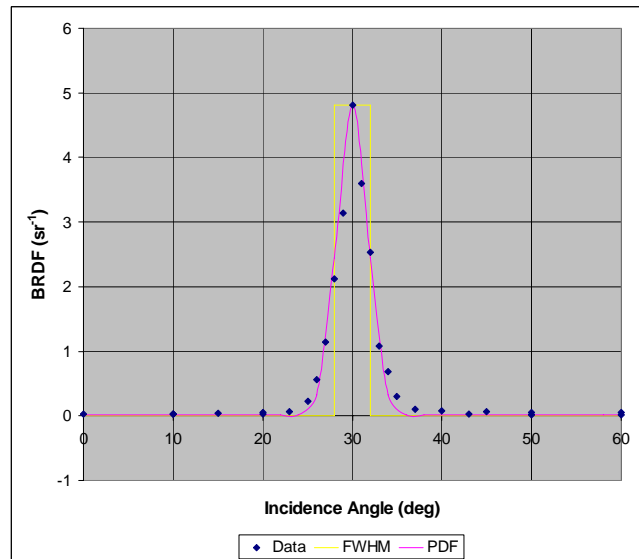


Figure 4: Bi-directional reflectance versus incidence for a 10µm source positioned in-plane at 30°.

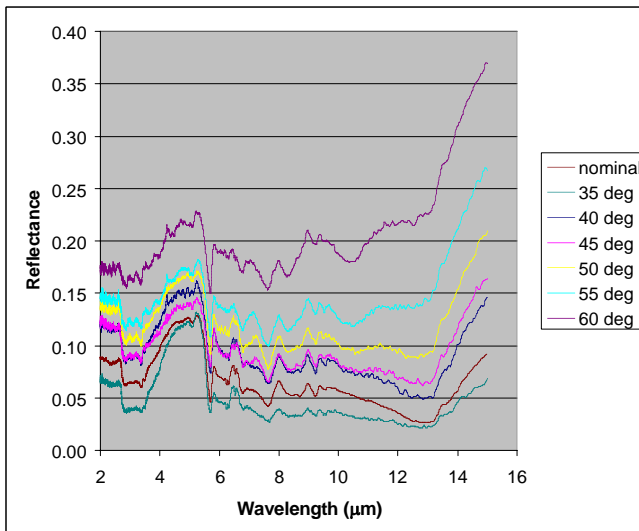


Figure 5: Surface reflectance versus wavelength for a range of incidence angles.

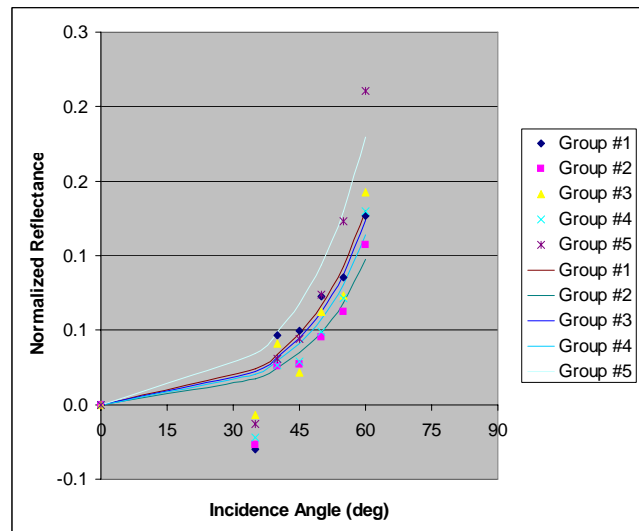


Figure 6: Fitting of S-R model to Quest measurements for different spectral groupings of reflectance.

2.3 ShipIR model

The surface reflectance in ShipIR model is based on a 4-parameter model similar to that of Sandford and Robertson (1985). The total reflectance is assumed to be the arithmetic sum of a diffuse component (ρ_D) and a specular component (ρ_S), which are both wavelength dependent:

$$\rho(\theta, \lambda) = \rho_D(\lambda) + \rho_S(\theta, \lambda) \quad (6)$$

The most significant contribution from Sandford and Robertson was the partition of surface reflectance into mutually exclusive spectral and angle-dependent terms:

$$\rho_S(\theta, \lambda) = g(\theta) \cdot \rho_S(0, \lambda) + [1 - g(\theta)] \cdot [1 - \rho_D(\lambda)] \quad (7)$$

The grazing-angle term (g) is defined as:

$$g(\theta) = \frac{1}{1 + b \cdot \tan^2 \theta} \quad (8)$$

The normalized reflectance data previously shown in Figure 6 is defined as $1-g(\theta)$ and is plotted in Figure 7 for b ranging from 10^{-7} to 0.10. The ShipIR definition of b differs from that of Sandford and Robertson by:

$$b_{SHIPIR} = \sqrt{b_{SR}} \quad (9)$$

Values of b obtained for the five spectral groups in Figure 6 are shown in Table 1 for the Quest yellow and white paints. Similar values are obtained for both paints in the same spectral group, but a 50% variation in b occurs across the infrared spectrum. Based on the average value of b in Table 1, the RMS difference between the FFI measurements and the model are within 2% for the 3–5 and 8–11 μm bands, and 2 to 10% in the 11–15 μm band – a factor to be considered when using the Quest ShipIR model to predict signatures beyond 11 μm .

The remaining components of the ShipIR surface reflectance pertain to the bi-directional reflection geometry. The following methods are used to define the radiance associated with a non-glint (sea, sky or secondary ship) source:

- The observer line-of-sight is computed relative to the ship surface ($\phi_{\text{obs}}, \theta_{\text{obs}}$) and used to determine the centre of the specular lobe ($\phi_i = \phi_r + \pi = \phi_{\text{obs}} + \pi$ and $\theta_r = \theta_i = \theta_{\text{obs}}$).
- The resultant incident angle (θ) is used to compute the specular reflectance based on Equation 6.

A dirac delta function is then used to determine which point-source (sun, sea-glint) if any is within the specular lobe-width of the coating:

$$\rho = \begin{cases} 0 & \vec{n}_i \cdot \vec{n}_s < \cos\left(\frac{e_{lobe}}{2}\right) \\ \rho(\theta, \lambda) & \vec{n}_i \cdot \vec{n}_s \geq \cos\left(\frac{e_{lobe}}{2}\right) \end{cases} \quad (10)$$

e_{lobe} denotes the 4th and last parameter in the ShipIR reflectance model – the full width at half maximum (FWHM) as shown in Figures 3 and 4.

2.4 Other BRDF models

More definitive BRDF models have been developed based on surface roughness, such as that by Ward (1992):

$$L_r(\phi_r, \theta_r) = \int_0^{2\pi} \int_0^{\pi/2} \rho_{bd}(\phi_i, \theta_i, \phi_r, \theta_r) L_i(\phi_i, \theta_i) \cos \theta_i \sin \theta_i d\phi_i d\theta_i \quad (11)$$

$$\rho_{bd}(\phi_i, \theta_i, \phi_r, \theta_r) = \frac{\rho_D}{\pi} + \frac{\rho_S}{\sqrt{\cos \theta_r \cos \theta_i}} \cdot \frac{\exp\left[-\left(\tan^2 \delta\right) / \sigma^2\right]}{4\pi\sigma^2} \quad (12)$$

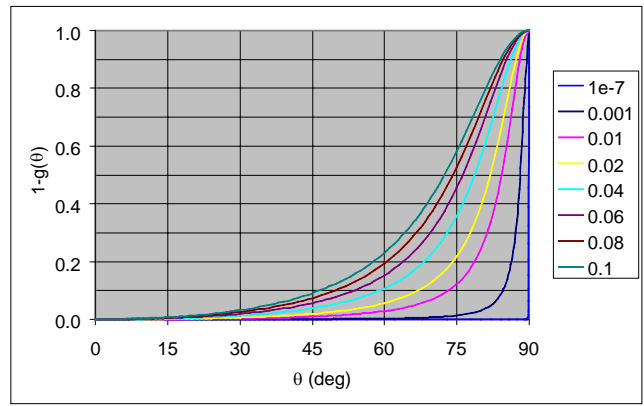


Figure 7: Normalized reflectance versus incidence angle (θ) for different values of b_{SHIPIR} .

Table 1: b parameters obtained for the Quest paints using the FFI measurements.

λ_k	b_k	
	yellow paint	white paint
2.0–2.7	0.048	0.050
2.7–3.5	0.036	0.036
3.5–5.7	0.065	0.047
5.7–10.7	0.044	0.043
10.7–15.0	0.075	0.073
average	0.051	0.047

This model has been shown to inadequately represent bi-directional reflectance at high angles of incidence because of the cosine terms in Equation 12, and its retention of a BRDF (sr^{-1}) in Equation 11. When comparing the Ward radiance equation with that of Cox and Munk (1954):

$$L_r(\phi_r, \theta_r) = \int_{-\infty}^{+\infty} \int_{-\infty}^{+\infty} L_i(\phi_i, \theta_i) \frac{\rho_s(\mu)}{2\pi\sigma_x\sigma_y} \cdot \exp\left[-\frac{m_x^2}{2\sigma_x^2} - \frac{m_y^2}{2\sigma_y^2}\right] dm_x dm_y \quad (13)$$

there are obvious similarities in the definition of roughness when the surface is assumed to be isotropic:

$$\tan \delta = \sqrt{m_x^2 + m_y^2} \quad (14)$$

$$\sigma_x = \sigma_y = \sigma \quad (15)$$

However, the Gaussian form of the probability density function (PDF) for surface roughness must be evaluated as a function of slope and not observer angle. As shown in Equation 13, the reflectance and radiance are integrated over the slope domain of reflection, which means the solid-angle subtended by both the source and detector must be mapped to a domain in surface slope; the resultant PDF integral alone provides a pseudo reflectance value with no units. The resultant formulation does have two important advantages: by definition, the total reflected energy is conserved

$$\int_{-\infty}^{+\infty} \int_{-\infty}^{+\infty} p(m_x, m_y) dm_x dm_y \equiv 1 \quad (16)$$

and there are no cosine terms in the reflectance nor surface radiance integral, since each micro-facet is assumed to be at the specular lobe angle ($\phi_r = \phi_i + \pi$, $\theta_r = \theta_i$) along a given slope vector (m_x, m_y, δ), as illustrated in Figure 8. The incidence angle to each micro-facet (μ_s) can also be different from the incidence angle to the average surface (θ_{obs}), depending on the actual value of surface roughness.

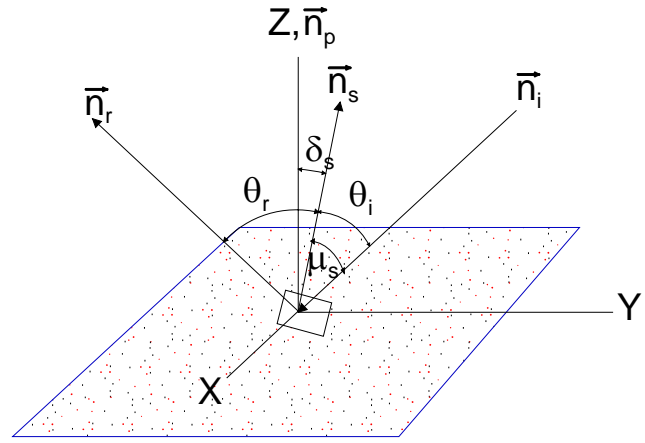


Figure 8: nomenclature for reflection off a rough surface.

3. SIMULATION STUDY

The following section describes an experiment conducted during the Q280 measurement trial to capture the solar-glint off Quest in the mid-wave and long-wave IR bands. These measurements allows us to evaluate the effects of paint and ship construction on surface BRDF and solar-glint. The results were presented during the workshop as four separate digital image sequences – one for each of the two IR band measurements, and one for each of the two IR band predictions using ShipIR. The methodology used to generate the ShipIR input data and construct the image sequence is described, and a few selected images taken at key time intervals are used to provide a qualitative comparison.

3.1 Trajectory data

Figure 9 shows a navigational chart of the waters near Halifax where the Q280 and other Quest trials were performed. As shown on the left side of the chart, the solar-glint measurements were obtained towards the end of the day on February 17, 2004 when two RCS measurement runs were executed. The solar azimuth and elevation angles were 247° and 5° , respectively, providing ideal conditions for a solar-glint reflection off the nearly vertical surfaces of the Quest. The ship was operating on its port-bow thruster, performing a 450° clockwise turn from its initial heading of 315° (facing the shore site). The blue circle indicates the area of the trajectory where the solar-glints occurred at relatively close range (830–930m). The GPS position and ship heading were recorded by the Quest at one minute intervals, and translated into ship relative position (azimuth, range) to the camera. The trajectory data were interpolated at one second intervals to provide the inputs to ShipIR, reproducing the IR camera recordings taken at 0.5 second intervals. The resultant time history of the raw and interpolated data are shown in Figures 10, 11, and 12 for ship heading, relative azimuth, and range, respectively.

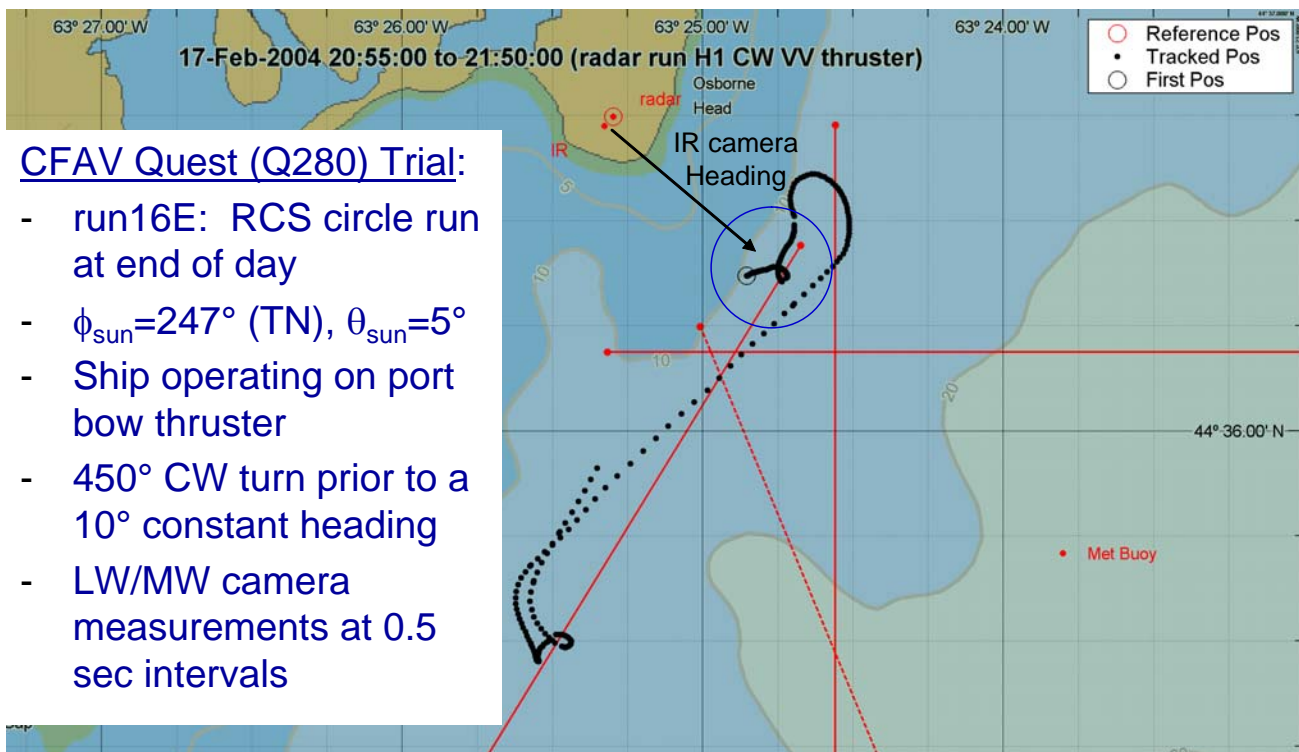


Figure 9: Navigational chart showing GPS location of IR camera and trajectory history of Quest during a RCS circle run.

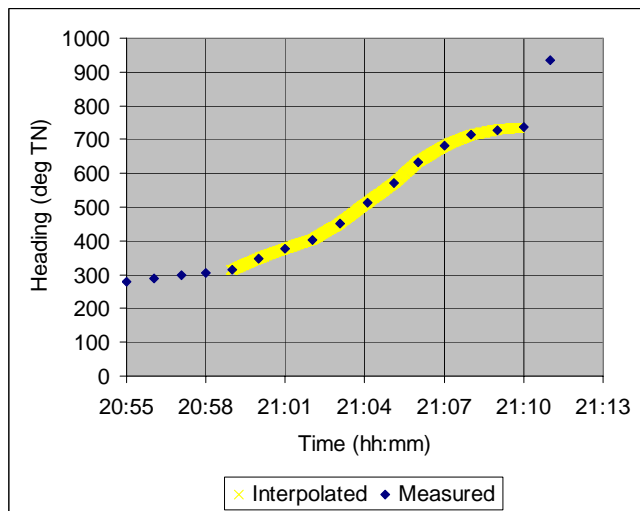


Figure 10: Ship heading versus time.

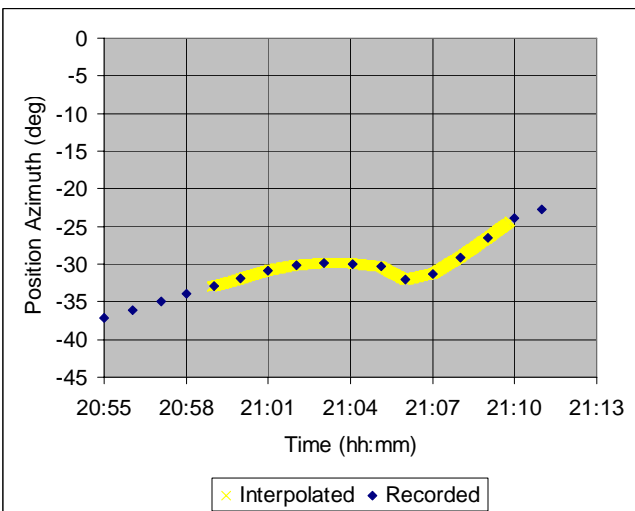


Figure 11: Relative azimuth of the ship (deg N of E) versus time.

The relative azimuth position is in polar coordinates (deg N of E), which differs from the true bearing (deg E of N) by an amount equal to $90-\alpha$. To avoid sharp discontinuities in the interpolated results around the transition from 360° to 0° , ship headings were incremented by 360° after each circle (360° , 720° , etc.). The interpolated results were fed into ShipIR using an I/O Library that allows users to create customized applications for controlling the execution of ShipIR via a standard set of script commands issued through shared-memory. The rendered output from ShipIR is either captured back through shared memory (as binary image data) or stored to file using the ShipIR shell script command to execute the `import` command (under Linux). The indexed output image files are encoded into .mpeg or .avi output files using a Linux video stream processing command called `transcode`.

3.2 Glint sequences

Figures 13 through 32 show the various measured and predicted images taken at key time intervals during glint measurement and simulation. The first set of images were taken at 21h:00:34 where a solar-glint occurs mid-ship off the port side. The ship is positioned at 121.3° (TN) and the solar azimuth is 247.15° (TN) so the port-side facet normals bisect the azimuth angles of the camera and sun for ship headings of 4.2+/-1.7° (TN). The full-width at half-maximum of the Quest white and yellow paints is 3.4°. The interpolated ship heading for this first sequence is 5.3° (TN). The measured glint in the 3–5µm band appears to cover a wider area of the ship, both forward and upward, including the yellow surfaces of the funnel, compared to the ShipIR predicted image. The long-wave (8–12µm) measured and predicted images are used to help discriminate between areas of thermal emission and solar-glint reflection. There is no measurable solar emission or reflection in the 8–12µm band.

Figure 13 also shows the presence of a ship *halo*, the ship's reflection off the ocean just below the waterline, which is also more acute in the vicinity of the solar-glint reflection. The halo effect is not yet modelled by ShipIR. The second glint sequence at 21h:03:05 shows the Quest positioned at 299.9° (TN) with a heading of 93.6°; the aft portions of the ship are now oriented at the half-angle between the camera and solar azimuth. The predicted results in Figure 19 appear to cover more surface area than the measurement and warrant further analysis. The next glint sequence occurs off the starboard facets at 21h:04:37 with the ship positioned at 300.2° (TN) and a heading of 183.3°. Similar to the port side, a larger glint area is shown in the measured image, both forward and upward, and the ship *halo* is also seen off the ocean just below the ship. The fourth glint sequence is taken at 21h:06:03 where a line or band of solar-glint travels across the front of the bridge. The ship is positioned at 302.1° with a heading of 276.4°; facets facing 274.6° would be in the half-angle between the camera and solar azimuth. The angles and positions noted above are from the GPS recorded by the ship and calculated using the axis origin of the ship geometry. The distance between the origin and a particular facet, and the distance between the origin and the GPS antennae location could account for small differences in angle between the ship heading and the actual position of a solar-glint on the ship surface. The final set of images were captured as the Quest proceeded to exit the RCS circle at 21h:08:32. The ship is positioned at 297.7° with a heading of 1.8° (TN); the port-side surfaces are once again oriented along the half-angle between the camera and solar azimuth.

One visible difference between the measurement and predictions is the discrete nature of the simulated glint. The dirac delta function used to compute the solar-glint term in the radiance equation is one obvious source, but the effect of optical blur from the camera is also responsible for some of the point-spread in the measured images. The following section explores other issues and ideas on how ShipIR can be further improved to deal with non-uniformities present in actual IR images.

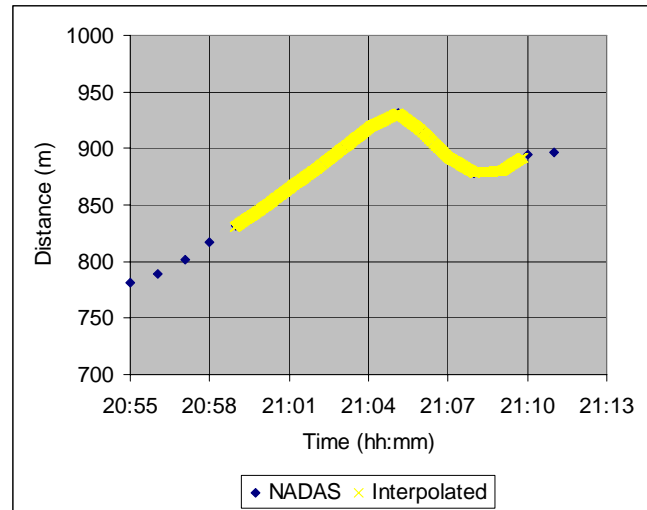


Figure 12: Distance to the ship versus time.

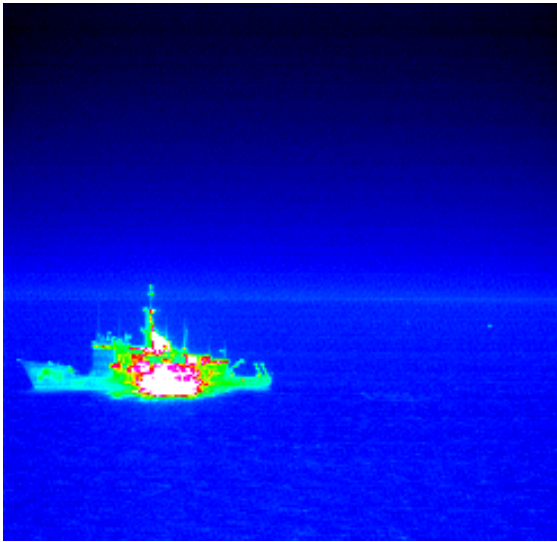


Figure 13: 3–5 μm measurement at 21h:00:34.

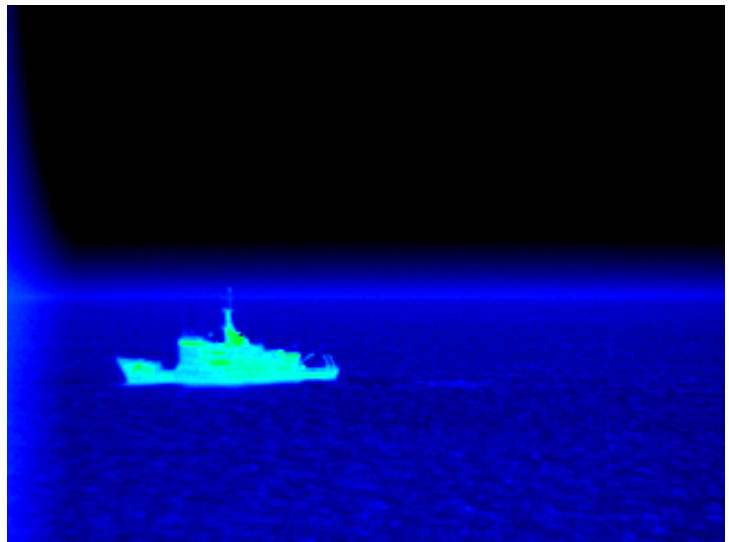


Figure 14: 8–12 μm measurement at 21h:00:34.



Figure 15: 3–5 μm prediction at 21h:00:34.

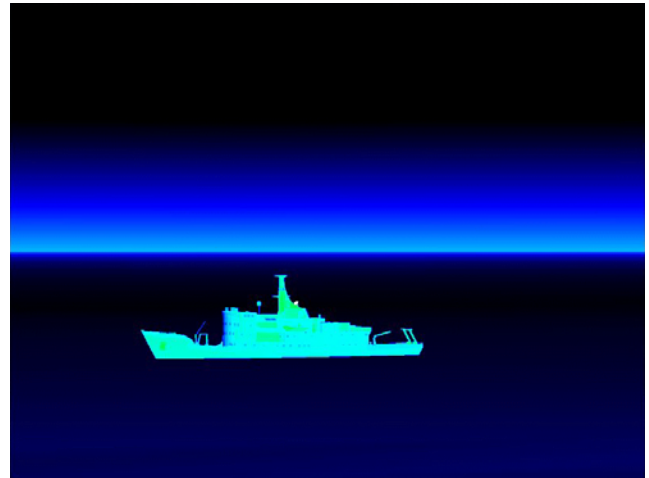


Figure 16: 8–12 μm prediction at 21h:00:34.

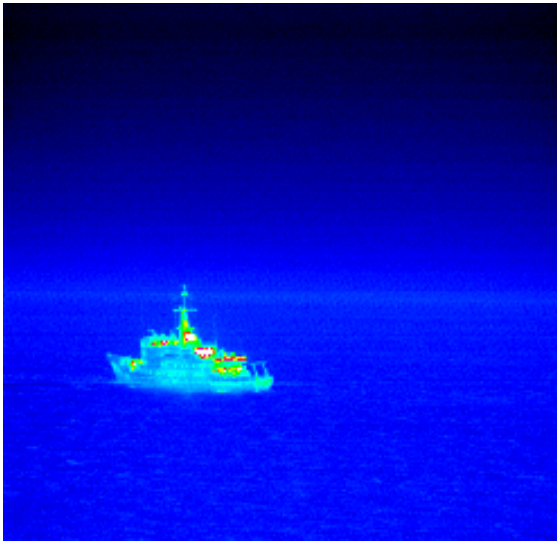


Figure 17: 3–5 μm measurement at 21h:03:05.

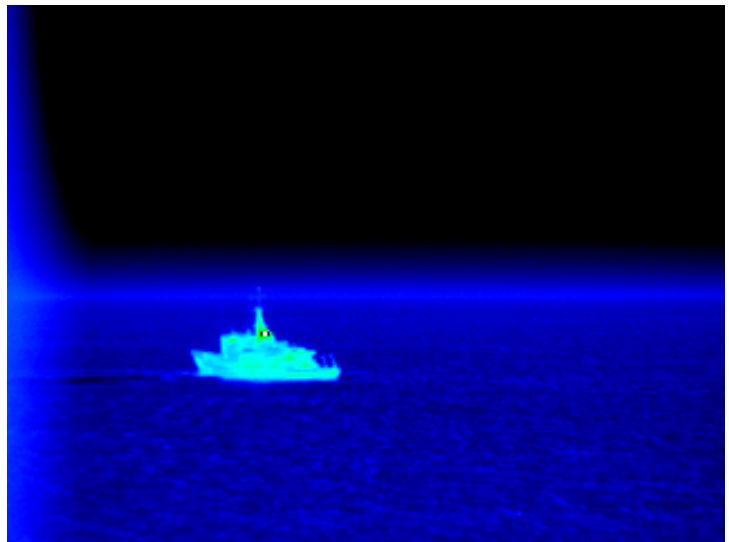


Figure 18: 8–12 μm measurement at 21h:03:05.

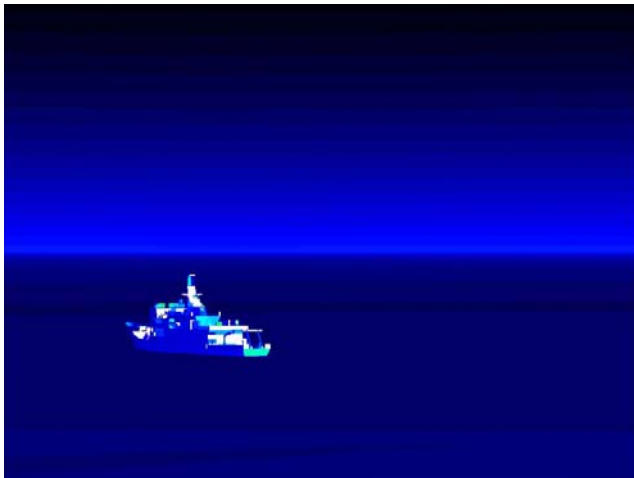


Figure 19: 3–5 μm prediction at 21h:03:05.

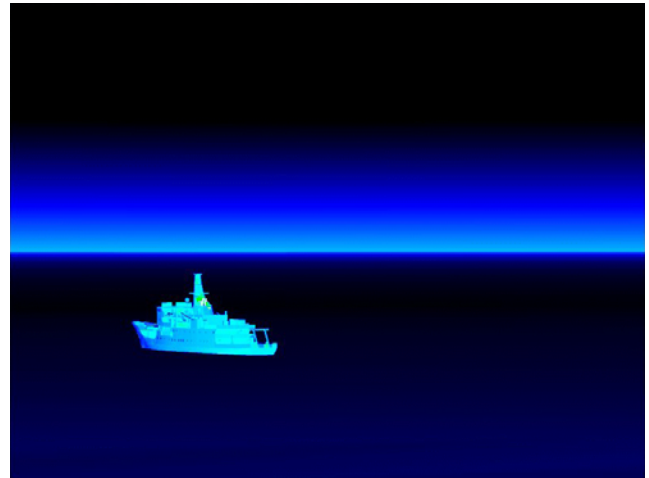


Figure 20: 8–12 μm prediction at 21h:03:05.

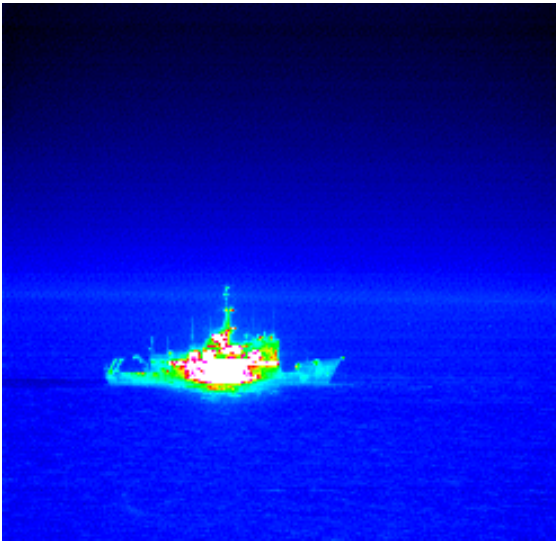


Figure 21: 3–5 μm measurement at 21h:04:37.

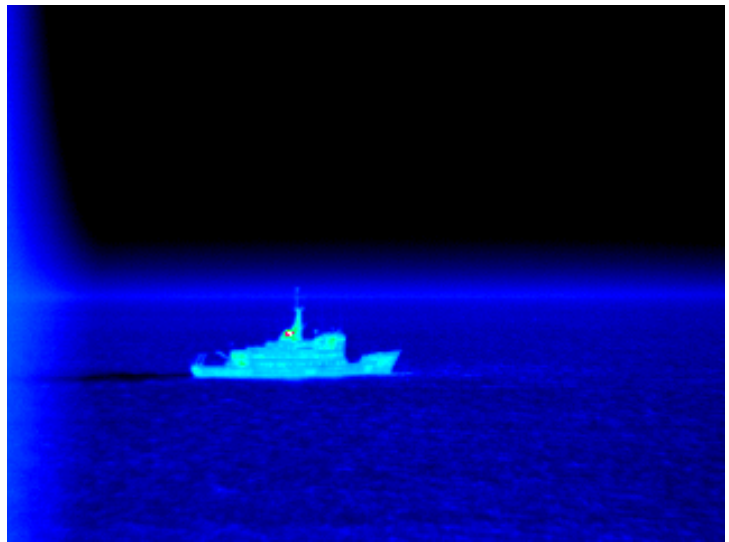


Figure 22: 8–12 μm measurement at 21h:04:37.



Figure 23: 3–5 μm prediction at 21h:04:37.

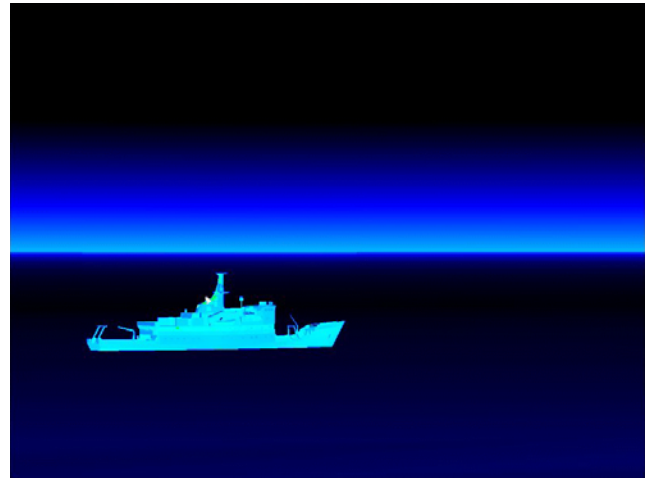


Figure 24: 8–12 μm prediction at 21h:04:37.



Figure 25: 3–5 μm measurement at 21h:06:03.



Figure 26: 8–12 μm measurement at 21h:06:03.



Figure 27: 3–5 μm prediction at 21h:06:03.



Figure 28: 8–12 μm prediction at 21h:06:03.

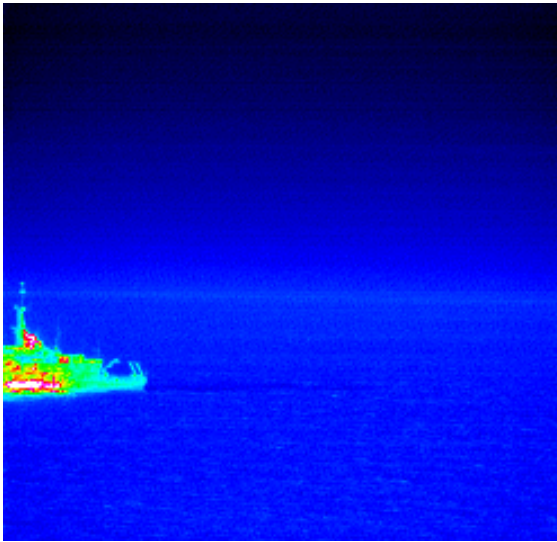


Figure 29: 3–5 μm measurement at 21h:08:32.

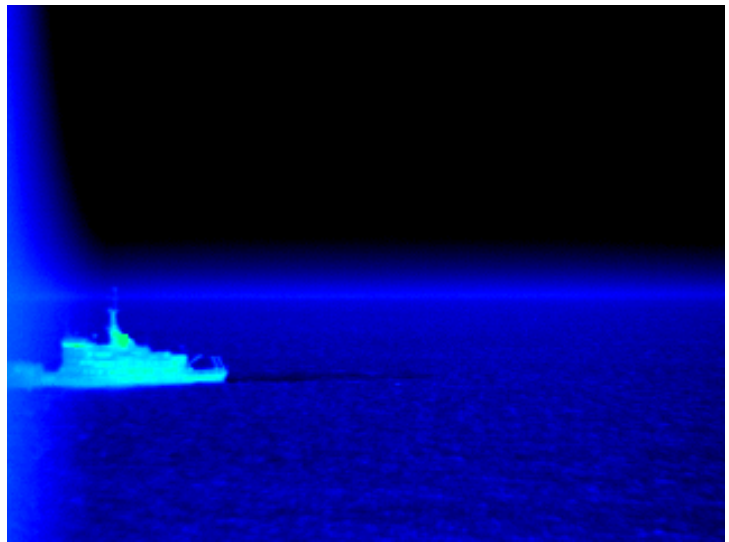


Figure 30: 8–12 μm measurement at 21h:08:32.



Figure 31: 3–5 μm prediction at 21h:08:32.



Figure 32: 8–12 μm prediction at 21h:08:32.

4. DISCUSSION

Another feature of ship geometry that can have a significant impact on specular lobe properties of the surface is the curvature introduced by ship construction techniques. The use of stiffeners and additional welds to strengthen warships and reduce weight and cost can cause a secondary or macro level surface roughness referred to by some Navies as the *hungry horse* effect. The impact of these large scale curvatures is not currently measured because of the uniformity and small size of paint samples used to measure optical properties. As shown in Figure 33, a grey-level histogram generated from a flat area on the photographed ship, denoted by the red curve, reveals that reflected sunlight off large scale surface distortions follows a Gaussian distribution, similar to the BRDF lobe of the paint. These macro geometry effects could be modelled by a pseudo-roughness value larger than the value obtained from optical surface property measurements. The actual value of surface roughness can only be obtained through direct measurement and modelling of the whole ship, as described in this paper.

This paper has reviewed the definitions, measurements and modelling techniques associated with bi-directional reflectance. The ship surface and sea reflectance models of ShipIR have been described, showing how various definitions and measurements are implemented to create an operational IR signature model of a vessel. The sample simulations and comparisons against the Q280 IR solar-glint measurement require further quantitative analysis to determine the absolute accuracy of the ShipIR surface reflectance model, and identify potential improvements. The measurement of mid-wave solar-glint provides one possible method to quantify the full-scale BRDF of the ship platform, including any pseudo-roughness introduced by the ship construction techniques. Future development of ShipIR will include an upgrade to the existing specular lobe model based on the surface roughness model already included in the sea reflectance model. The ship surface radiance and IR rendering models will also be upgraded to use two-dimensional texture mapping to capture the effect of pseudo-roughness on large faceted areas of the ship. We hope to present the results of this ongoing work at a future ITBM&S workshop.

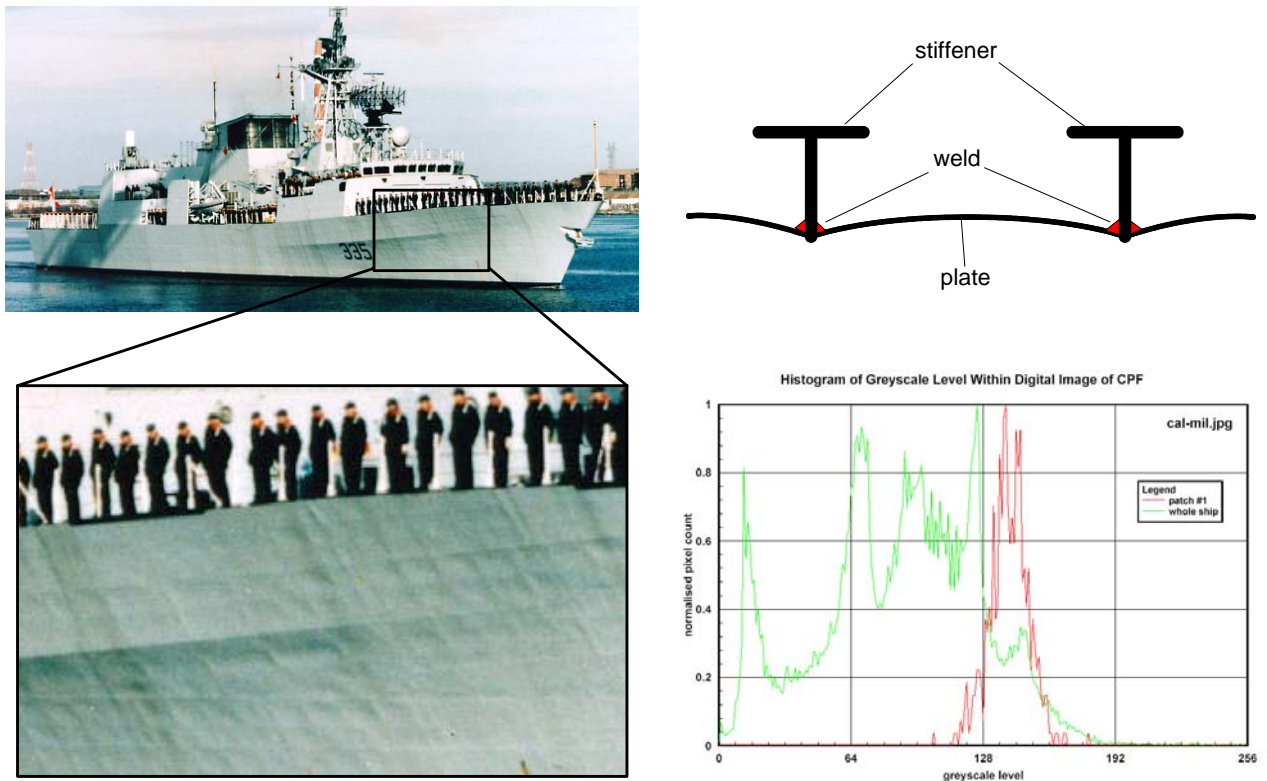


Figure 33: Visual photograph and histogram illustrating the macro roughness introduced by ship construction.

5. REFERENCES

1. Cox, C. and W. Munk. 1954. Measurement of the Roughness of the Sea Surface from Photographs of the Sun's Glitter, *J. Opt. Society Am.* 44, p. 838-850.
2. Fraedrich, D.S., E. Stark, L.T. Heen and C. Miller. 2003. ShipIR model validation using NATO SIMVEX experiment results. *Proc. SPIE* 5075:49-59, Targets and Backgrounds IX: Characterization and Representation.
3. Mermelstein, M.D., E.P. Shettle, E.H. Takken and R.G. Priest. 1994. Infrared radiance and solar glint at the ocean-sky horizon. *Appl. Opt.* 33 (25):6022-6034.
4. Sandford, B.P. and D.C. Robertson. 1985. Infrared reflectance properties of aircraft paints (U). *Proc. IRIS: Targets, Backgrounds, and Discrimination*.
5. Ship and Atmospheric Propagation Phenomena Infrared Experiment (SAPPHIRE), NATO SET/088 RTG51 on Littoral Infrared Ship Self Defence Technology, June 2006, Chesapeake Bay, USA.
6. Vaitekunas, D.A. and D.S. Fraedrich. 1999. Validation of the NATO-standard ship signature model (SHIPIR). *Proc. SPIE* 3699: 103-113, Targets and Backgrounds: Characterization and Representation V.
7. Vaitekunas, D.A. 2004. *Infrared Signature Instrumentation, Measurement, and Modelling of CFAV Quest for Trial Q276*. Davis Document No. A320-001, Rev 0 (performed under PWGSC Contract No. W7707-3-2128).
8. Vaitekunas, D.A. 2005. Validation of ShipIR (v3.2): methods and results. Presented at *1st International Workshop for IR Target and Background Modelling*, 27–30 June, 2005. Ettlingen, Germany.